

The role of diffraction in the Casimir effect beyond the proximity force approximation

VINICIUS HENNING^{1,*}, BENJAMIN SPRENG^{1,2}, MICHAEL HARTMANN², GERT-LUDWIG INGOLD², AND PAULO A. MAIA NETO¹

¹Instituto de Física, Universidade Federal do Rio de Janeiro, CP 68528, Rio de Janeiro RJ 21941-909, Brazil

²Universität Augsburg, Institut für Physik, 86135 Augsburg, Germany

*Corresponding author: henning@if.ufrj.br

Compiled September 8, 2021

We derive the leading-order correction to the proximity force approximation (PFA) result for the electromagnetic Casimir interaction in the plane-sphere geometry by developing the scattering approach in the plane-wave basis. Expressing the Casimir energy as a sum over round trips between plane and sphere, we find two distinct contributions to the correction. The first one results from the variation of the Mie reflection operator, calculated within the geometric optical WKB approximation, over the narrow Fourier interval associated to specular reflection at the vicinity of the point of closest approach on the spherical surface. The second contribution, accounting for roughly 90% of the total correction, results from the modification of the geometric optical WKB Mie scattering amplitude due to diffraction. Our derivation provides a clear physical understanding of the nature of the PFA correction for spherical surfaces.

<http://dx.doi.org/10.1364/ao.XX.XXXXXX>

1. INTRODUCTION

The Casimir interaction between material surfaces is a striking consequence of the quantum nature of electrodynamics [1]. The plane-sphere geometry is particularly suited to implement very precise measurements of the Casimir force or force gradient [2–5]. The interaction for such geometry has been probed for a number of different materials over the last decade [6–12]. The Casimir interaction between two spherical surfaces is also of great interest [13–15] given its applications in colloids and surface sciences [16].

Until recently, the theoretical description of plane-sphere experiments has been limited to the employment of the proximity force approximation (PFA), also known as Derjaguin approximation [17]. Within PFA, the Casimir energy is obtained from Lifshitz's formula for parallel planes by averaging over the local distance between the surfaces [18]. PFA provides the correct leading asymptotics for large sphere radius R when considering general materials and arbitrary temperatures [19]. As reviewed in [20], typical experiments are close to the validity range of PFA since they correspond to aspect ratios $R/L > 10^2$, where L is the minimal distance between the surfaces as indicated in Fig. 1. Nevertheless, it is still necessary to access the accuracy of this approximation when comparing with experimental data. Early attempts [21–26] to derive exact numerical results from the scattering approach [27, 28] were limited to moderate values of R/L . Results for typical experimental conditions were finally derived by developing the scattering operator describing a round trip

between plane and sphere in a symmetrical form [20, 29].

Analytical results complement the numerical work by bringing information on the nature of PFA and its leading-order correction. In a previous paper [19], we have shown that the PFA result for the interaction between two spheres is obtained by taking the geometric optical WKB Mie scattering amplitude and using the saddle-point approximation when computing multiple round trips between the two surfaces. The saddle point corresponds to the condition of specular reflection at the tangent plane to the sphere at the point of closest approach. In this paper, we show that the leading-order correction to PFA for the plane-sphere geometry results from two independent effects. The largest contribution arises from diffraction, which corrects the WKB scattering amplitude taken at the saddle point. The second contribution results from the correction to the saddle-point approximation. It accounts for the variation of the geometric optical WKB reflection operator within the narrow interval defined by the condition of specular reflection at the vicinity of the point of closest approach.

We develop the scattering formula [27, 28] in the plane-wave basis and expand the Casimir energy as a sum over multiple round trips between plane and sphere, which is computed analytically for large values of R/L . As opposed to semiclassical derivations in the position representation [30–32], the vicinity of the PFA regime defines a narrow interval in Fourier (momentum) space, thus allowing us to employ a saddle-point approach. Moreover, the momentum representation provides a direct con-

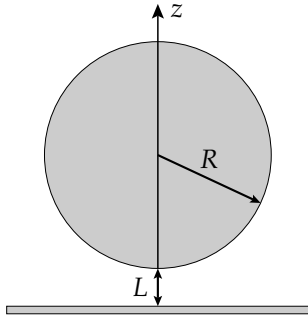


Fig. 1. Sphere of radius R and plate separated by a distance L .

nection with the geometrical optics picture and allows for the use of known results in semiclassical optics [33, 34]. For simplicity, we consider perfect metals at zero temperature, but the extension to real materials would be straightforward.

Previous derivations of the leading-order correction for the scalar [35] and electromagnetic [36] field models were based on asymptotic approximations in the multipolar basis. Alternatively, the derivative expansion approach also allows for the derivation of the scalar [37] and electromagnetic [38] results. Real materials at zero temperature were also investigated within the multipolar [39] and derivative [40] approaches. A non-trivial dependence on L/R was found for finite temperatures [41–44], depending on the field model and material properties.

The paper is organized in the following way. In Section 2, we present the basic tools for developing the scattering formula in the plane-wave basis. Section 3 is dedicated to the Mie reflection operator and its semiclassical expansion. The two contributions to the leading-order correction to PFA are derived in Section 4 and concluding remarks are presented in Section 5. Some technical aspects of our calculation are relegated to the Appendix.

2. CASIMIR ENERGY IN THE PLANE-WAVE BASIS

In this section, we develop the scattering formula for the Casimir energy in terms of the plane-wave basis. We consider a sphere and a plate as indicated in Fig. 1. We have chosen the z -axis as the axis of symmetry while the plate lies in the xy -plane. The distance between the sphere's center and the plate is given by $L + R$.

The plane-wave basis for the electromagnetic field is characterized by the wave vector $\mathbf{K} = (K_x, K_y, K_z)$ and the polarization p . In the region between sphere and plate which we assume to be vacuum, the frequency of the plane wave is determined by means of the dispersion relation $\omega = c|\mathbf{K}|$ where c is the vacuum speed of light.

As the frequency of a plane wave remains unchanged during a round trip between sphere and plate, it is convenient to employ the so-called angular spectral representation [45]. Here, the three-dimensional wave vector \mathbf{K} is replaced by the frequency ω and the two-dimensional projection $\mathbf{k} = (K_x, K_y, 0)$ onto the xy -plane. Since ω and \mathbf{k} only allow to determine the modulus of K_z , we need to introduce the sense of propagation along the z -axis, $\phi = \pm 1$, so that

$$K_z = \phi k_z \quad (1)$$

with

$$k_z = \left(\frac{\omega^2}{c^2} - \mathbf{k}^2 \right)^{1/2}. \quad (2)$$

A basis state within the angular spectral representation is then denoted as $|\omega, \mathbf{k}, p, \phi\rangle$.

The polarization p is either transverse electric (TE) or transverse magnetic (TM) with respect to the Fresnel plane spanned by the vectors \mathbf{K} and $\hat{\mathbf{z}}$, with the latter defining the normal to the planar surface. The polarization unit vectors are then defined by

$$\begin{aligned} \hat{\mathbf{e}}_{\text{TE}} &= \frac{\hat{\mathbf{z}} \times \hat{\mathbf{K}}}{|\hat{\mathbf{z}} \times \hat{\mathbf{K}}|} \\ \hat{\mathbf{e}}_{\text{TM}} &= \hat{\mathbf{e}}_{\text{TE}} \times \hat{\mathbf{K}} \end{aligned} \quad (3)$$

with the unit vector $\hat{\mathbf{K}} = \mathbf{K}/|\mathbf{K}|$.

In the position representation a plane wave is now given by

$$\langle x, y, z | \omega, \mathbf{k}, p, \phi \rangle = \hat{\mathbf{e}}_p \left(\frac{1}{2\pi} \left| \frac{\omega}{ck_z} \right| \right)^{1/2} \exp[i(\mathbf{k} \cdot \mathbf{r} + \phi k_z z)] \quad (4)$$

where $\mathbf{r} = (x, y, 0)$ is the projection of the position vector onto the xy -plane. The normalization prefactor is specific for the angular spectral representation.

Within the scattering approach to the Casimir effect, it is convenient to express the Casimir energy in terms of the imaginary frequency $\zeta = -i\omega$ and to introduce an imaginary wave vector component along the z -direction, $\kappa = -ik_z$. The corresponding dispersion relation reads

$$\zeta^2 = c^2(\kappa^2 - \mathbf{k}^2). \quad (5)$$

At zero temperature, the Casimir energy is then found as an integral over imaginary frequencies [27, 28]:

$$\mathcal{E} = \hbar \int_0^\infty \frac{d\zeta}{2\pi} \text{tr} \log(1 - \mathcal{M}(\zeta)). \quad (6)$$

Here, \mathcal{M} is an operator describing the round trip of a wave between the objects involved. For our geometry consisting of a sphere and a plate as shown in Fig. 1, we specifically have

$$\mathcal{M} = \mathcal{T}_{\text{PS}} \mathcal{R}_{\text{S}} \mathcal{T}_{\text{SP}} \mathcal{R}_{\text{P}}. \quad (7)$$

\mathcal{R}_{S} and \mathcal{R}_{P} describe reflection at sphere and plate, respectively. The operators \mathcal{T}_{SP} and \mathcal{T}_{PS} perform a translation over a distance $L + R$ along the positive and negative z direction, respectively. They are needed to perform the transition between a reference frame situated at the sphere center and another reference frame with the origin on top of the plate.

Within the plane-wave basis, the translation operators \mathcal{T}_{PS} and \mathcal{T}_{SP} are diagonal, contributing a factor $\exp(-\kappa(L + R))$ each. The reflection operator \mathcal{R}_{P} at the plate is diagonal as well with matrix elements given by the Fresnel coefficients when taking the polarization basis defined by (3). For the case of perfect reflectors considered here, the matrix elements correspond to the reflection coefficients $r_{\text{TM}} = 1$ and $r_{\text{TE}} = -1$.

The Mie reflection operator \mathcal{R}_{S} at the sphere requires more attention because it couples different polarizations and values of \mathbf{k} . The detailed form of the corresponding matrix elements will be discussed in Section 3.

We make the Casimir energy (6) amenable to an analytical treatment by expanding the logarithm into a Mercator series

$$\mathcal{E} = -\hbar \sum_{r=1}^{\infty} \frac{1}{r} \int_0^\infty \frac{d\zeta}{2\pi} \text{tr} \mathcal{M}^r \quad (8)$$

which physically implies a decomposition into terms with a specific number r of round trips between sphere and plane. In the plane-wave representation, the trace reads

$$\text{tr } \mathcal{M}^r = \sum_{p_0, \dots, p_{r-1}} \int \frac{d\mathbf{k}_0 \dots d\mathbf{k}_{r-1}}{(2\pi)^{2r}} \prod_{j=0}^{r-1} e^{-2\kappa_j(L+R)} r_{p_j} \times \langle \mathbf{k}_{j+1}, p_{j+1}, - | \mathcal{R}_S | \mathbf{k}_j, p_j, + \rangle \quad (9)$$

where we sum over all intermediate polarizations p_j with corresponding reflection coefficients r_{p_j} and integrate over all intermediate values of the transversal wave vector \mathbf{k}_j . Here and in the following, we use a cyclic index convention where $j = r$ is equivalent to $j = 0$.

3. SCATTERING AT THE SPHERE

A. Exact matrix elements

The remaining part to be specified in the decomposition of the Casimir energy (8) are the matrix elements of the reflection operator \mathcal{R}_S at the sphere. Because of our choice of the plane-wave basis, this operator is the only one appearing in the round-trip operator (7) leading to non-diagonal matrix elements.

An incident plane wave with wave vector $\mathbf{K}^{(\text{in})}$ will be scattered by a sphere into a superposition of plane waves with arbitrary wave vectors $\mathbf{K}^{(\text{out})}$. Here, we will consider a specific pair of incident and scattered wave vectors $\mathbf{K}^{(\text{in})}$ and $\mathbf{K}^{(\text{out})}$, respectively, which span the so-called scattering plane. As long as the plate is not part of the scattering geometry, it is advantageous to employ the polarization vectors with respect to the scattering plane defined as

$$\begin{aligned} \hat{\mathbf{e}}_{\perp} &= \frac{\hat{\mathbf{K}}^{(\text{out})} \times \hat{\mathbf{K}}^{(\text{in})}}{|\hat{\mathbf{K}}^{(\text{out})} \times \hat{\mathbf{K}}^{(\text{in})}|} \\ \hat{\mathbf{e}}_{\parallel}^{(\text{in})} &= \hat{\mathbf{e}}_{\perp} \times \hat{\mathbf{K}}^{(\text{in})} \\ \hat{\mathbf{e}}_{\parallel}^{(\text{out})} &= \hat{\mathbf{e}}_{\perp} \times \hat{\mathbf{K}}^{(\text{out})}. \end{aligned} \quad (10)$$

The polarization vector $\hat{\mathbf{e}}_{\perp}$ is used for, both, the incident and the scattered wave, while in general $\hat{\mathbf{e}}_{\parallel}$ points in different directions in the two scattering channels.

Since the polarization in the basis (10) is conserved during the scattering at a sphere, \mathcal{R}_S is block diagonal with matrix elements

$$\begin{aligned} \langle \mathbf{K}^{(\text{out})}, \perp | \mathcal{R}_S | \mathbf{K}^{(\text{in})}, \perp \rangle &= \frac{2\pi c}{\xi_{\mathbf{K}^{(\text{out})}}} S_{\perp} \\ \langle \mathbf{K}^{(\text{out})}, \parallel | \mathcal{R}_S | \mathbf{K}^{(\text{in})}, \parallel \rangle &= \frac{2\pi c}{\xi_{\mathbf{K}^{(\text{out})}}} S_{\parallel} \end{aligned} \quad (11)$$

where the scattering amplitudes are given by

$$S_{\perp} = \sum_{\ell=1}^{\infty} \frac{2\ell+1}{\ell(\ell+1)} [a_{\ell} \pi_{\ell}(\cos \Theta) + b_{\ell} \tau_{\ell}(\cos \Theta)] \quad (12)$$

$$S_{\parallel} = \sum_{\ell=1}^{\infty} \frac{2\ell+1}{\ell(\ell+1)} [a_{\ell} \tau_{\ell}(\cos \Theta) + b_{\ell} \pi_{\ell}(\cos \Theta)]. \quad (13)$$

Here, a_{ℓ} and b_{ℓ} are the Mie coefficients and the functions π_{ℓ} and τ_{ℓ} can be expressed in terms of Legendre polynomials and depend on the scattering angle defined through the relation

$$\cos(\Theta) = -\frac{c^2}{\xi^2} (\kappa^{(\text{in})} \kappa^{(\text{out})} + \mathbf{k}^{(\text{in})} \cdot \mathbf{k}^{(\text{out})}). \quad (14)$$

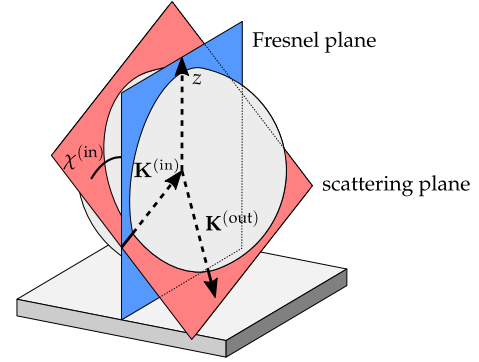


Fig. 2. The Fresnel plane for the incoming wave vector $\mathbf{K}^{(\text{in})}$ in general does not coincide with the scattering plane. The two planes are at an angle $\chi^{(\text{in})}$. The corresponding Fresnel plane for the outgoing wave vector $\mathbf{K}^{(\text{out})}$ is not shown.

The functions a_{ℓ} , b_{ℓ} , π_{ℓ} , and τ_{ℓ} are defined in Ref. [46]. For the purpose of our considerations, we will not need the explicit expressions.

So far, the matrix elements are expressed in the polarization basis (10) related to the scattering plane spanned by the vectors $\mathbf{K}^{(\text{in})}$ and $\mathbf{K}^{(\text{out})}$ as displayed in Fig. 2. In view of our sphere-plate geometry, it is more suitable to make use of the polarization basis (3) associated with the Fresnel plane spanned by the vectors $\mathbf{K}^{(\text{in})}$ and $\hat{\mathbf{z}}$ shown in Fig. 2, which is tilted by an angle $\chi^{(\text{in})}$ with respect to the scattering plane. Likewise, the Fresnel plane associated to the outgoing wave vector $\mathbf{K}^{(\text{out})}$ is tilted with respect to the scattering plane by an angle $\chi^{(\text{out})}$.

The comparison between the two polarization bases (3) and (10) allows us to connect the results (11) of the Mie theory with our sphere-plate scattering geometry. The matrix elements of \mathcal{R}_S in the Fresnel polarization basis (3) are given by

$$\langle \mathbf{k}^{(\text{out})}, \text{TM}, - | \mathcal{R}_S | \mathbf{k}^{(\text{in})}, \text{TM}, + \rangle = \frac{2\pi c}{\xi_{\mathbf{K}^{(\text{out})}}} (AS_{\parallel} + BS_{\perp}) \quad (15)$$

$$\langle \mathbf{k}^{(\text{out})}, \text{TE}, - | \mathcal{R}_S | \mathbf{k}^{(\text{in})}, \text{TE}, + \rangle = \frac{2\pi c}{\xi_{\mathbf{K}^{(\text{out})}}} (AS_{\perp} + BS_{\parallel}) \quad (16)$$

$$\langle \mathbf{k}^{(\text{out})}, \text{TM}, - | \mathcal{R}_S | \mathbf{k}^{(\text{in})}, \text{TE}, + \rangle = -\frac{2\pi c}{\xi_{\mathbf{K}^{(\text{out})}}} (CS_{\perp} + DS_{\parallel}) \quad (17)$$

$$\langle \mathbf{k}^{(\text{out})}, \text{TE}, - | \mathcal{R}_S | \mathbf{k}^{(\text{in})}, \text{TM}, + \rangle = \frac{2\pi c}{\xi_{\mathbf{K}^{(\text{out})}}} (CS_{\parallel} + DS_{\perp}). \quad (18)$$

The coefficients A , B , C , and D arise due to the fact that in general the scattering plane and the Fresnel planes do not coincide, as illustrated in Fig. 2. They can be cast into the form

$$\begin{aligned} A &= \cos(\chi^{(\text{out})}) \cos(\chi^{(\text{in})}) \\ B &= \sin(\chi^{(\text{out})}) \sin(\chi^{(\text{in})}) \\ C &= \sin(\chi^{(\text{out})}) \cos(\chi^{(\text{in})}) \\ D &= -\cos(\chi^{(\text{out})}) \sin(\chi^{(\text{in})}), \end{aligned} \quad (19)$$

where the angles between the Fresnel planes and the scattering plane are defined by the following relations

$$\begin{aligned} \cos(\chi^{(\text{in})}) &= \hat{\mathbf{e}}_{\text{TE}}(\mathbf{K}^{(\text{in})}) \cdot \hat{\mathbf{e}}_{\perp} \\ \cos(\chi^{(\text{out})}) &= \hat{\mathbf{e}}_{\text{TE}}(\mathbf{K}^{(\text{out})}) \cdot \hat{\mathbf{e}}_{\perp}. \end{aligned} \quad (20)$$

A special situation occurs when $\mathbf{K}^{(\text{out})}$ is contained in the Fresnel plane associated to $\mathbf{K}^{(\text{in})}$. In this case, the two Fresnel

planes coincide with the scattering plane and the angles $\chi^{(\text{in})}$ and $\chi^{(\text{out})}$ vanish. According to (20), we then find

$$A = 1, \quad B = C = D = 0. \quad (21)$$

In this case, the matrix elements (15)–(18) become diagonal and essentially reduce to the scattering amplitudes (12) and (13). It is this special scattering situation which dominates the Casimir energy within the proximity force approximation [19].

B. Scattering at large spheres

In order to derive the leading correction to the proximity force approximation, we need the asymptotic expansions of the exact matrix elements (15)–(18) valid for large R . The expansions for the scattering amplitudes S_{\perp} and S_{\parallel} are well known when taking real frequencies $\omega \gg c/R$ [47]. If the close vicinity of the forward direction is excluded, they are obtained within the WKB approximation.

It turns out that the asymptotic imaginary-frequency expression can be obtained by simply reexpressing the real-frequency expression in terms of imaginary frequencies [19]. The asymptotic scattering amplitudes including the leading correction in $1/R$ can be expressed as

$$S_p = S_p^{\text{WKB}} \left(1 + \frac{1}{R} s_p + \mathcal{O}(R^{-2}) \right). \quad (22)$$

Here, the leading WKB term is given by

$$S_p^{\text{WKB}} = (-1)^p \frac{\xi R}{2c} \exp \left[\frac{2\xi R}{c} \sin \left(\frac{\Theta}{2} \right) \right], \quad (23)$$

where the scattering angle Θ is given by (14), and $p = 1(2)$ stands for \perp (\parallel) polarization. The leading corrections in (22) in order $1/R$ are found as [34]

$$\begin{aligned} s_{\perp} &= \frac{c}{2\xi} \frac{\cos(\Theta)}{\sin^3(\Theta/2)} \\ s_{\parallel} &= -\frac{c}{2\xi} \frac{1}{\sin^3(\Theta/2)}. \end{aligned} \quad (24)$$

It should be noted that the leading-order term (23) in real frequencies has a clear interpretation in terms of geometrical optics [33]. While the proximity force approximation of the Casimir effect can thus be understood in terms of geometrical optics, the leading corrections derived here require us to take the diffraction correction (24) into account.

Plugging the asymptotic expansion of the scattering amplitudes (22) into the matrix elements (15)–(18), the asymptotic expansion of the matrix elements up to order $1/R$ can be summarized as

$$\begin{aligned} \langle \mathbf{k}^{(\text{out})}, p^{(\text{out})}, - | \mathcal{R}_S | \mathbf{k}^{(\text{in})}, p^{(\text{in})}, + \rangle \\ \simeq \frac{\pi R}{\kappa^{(\text{out})}} \exp \left[\frac{2\xi R}{c} \sin \left(\frac{\Theta}{2} \right) \right] \rho_{p^{(\text{out})}, p^{(\text{in})}} \end{aligned} \quad (25)$$

with

$$\begin{aligned} \rho_{\text{TM}, \text{TM}} &= (A - B) + \frac{1}{R} (As_{\parallel} - Bs_{\perp}) \\ \rho_{\text{TE}, \text{TE}} &= -(A - B) - \frac{1}{R} (As_{\perp} - Bs_{\parallel}) \\ \rho_{\text{TE}, \text{TM}} &= (C - D) + \frac{1}{R} (Cs_{\perp} - Ds_{\parallel}) \\ \rho_{\text{TM}, \text{TE}} &= (C - D) + \frac{1}{R} (Cs_{\parallel} - Ds_{\perp}). \end{aligned} \quad (26)$$

4. ASYMPTOTIC EXPANSION OF THE CASIMIR ENERGY

For large sphere radius, the Casimir energy can be expressed in the form

$$\mathcal{E} = \mathcal{E}_{\text{PFA}} \left(1 + \beta_1 \frac{L}{R} + o(R^{-1}) \right). \quad (27)$$

The well-known PFA result

$$\mathcal{E}_{\text{PFA}} = -\frac{\hbar c \pi^3 R}{720 L^2} \quad (28)$$

was shown to result from the leading order of a saddle-point evaluation of the round-trip decomposition (8) [19]. Here, we will focus on the evaluation of the constant β_1 .

There exist two sources for corrections of the order $1/R$ and we therefore write

$$\beta_1 = \beta_d + \beta_{\text{go}} \quad (29)$$

where the indices ‘d’ and ‘go’ refer to diffraction and geometrical optics, respectively. The first contribution, β_d , arises from the diffractive correction to the scattering amplitude, i.e. the term involving s_p in (22). The second contribution, β_{go} , is obtained by evaluating the saddle-point approximation to the next-to-leading order, referred to as NTLO in the following.

The central object for obtaining an asymptotic expansion of the Casimir energy is the trace (9) of the r -th power of the round-trip operator. Together with the asymptotic expansion of the matrix elements of \mathcal{R}_S (25), the trace can be brought into the form of the $2r$ -dimensional integral

$$\text{tr } \mathcal{M}^r \simeq \left(\frac{R}{4\pi} \right)^r \int d\mathbf{k}_0 \dots d\mathbf{k}_{r-1} g(\mathbf{k}_0, \dots, \mathbf{k}_{r-1}) e^{-Rf(\mathbf{k}_0, \dots, \mathbf{k}_{r-1})} \quad (30)$$

which is suitable for an evaluation using the saddle-point approximation. Here, we introduced the function

$$g(\mathbf{k}_0, \dots, \mathbf{k}_{r-1}) = \sum_{p_0, \dots, p_{r-1}} \prod_{j=0}^{r-1} (-1)^{p_j} \frac{e^{-2\kappa_j L}}{\kappa_j} \rho_{p_{j+1}, p_j}. \quad (31)$$

The factor $(-1)^{p_j}$ represents the Fresnel coefficient r_{p_j} for polarization $p_j = 1$ (TE) or $p_j = 2$ (TM), which accounts for reflection at the plate. The function in the exponent in (30) is given by

$$f(\mathbf{k}_0, \dots, \mathbf{k}_{r-1}) = \sum_{j=0}^{r-1} \eta_{j,j+1} \quad (32)$$

where

$$\eta_{j,j+1} = \kappa_j + \kappa_{j+1} - \left[2 \left(\frac{\xi^2}{c^2} + \kappa_j \kappa_{j+1} + \mathbf{k}_j \cdot \mathbf{k}_{j+1} \right) \right]^{1/2}. \quad (33)$$

While the first two terms in (33) are related to the translation from the sphere to the plate and back, the last term is associated to the phase upon reflection at the sphere within the WKB approximation.

A. Saddle-point approximation and its leading order correction

We will now derive the saddle-point approximation including the NTLO for the integrals (30). In the absence of relevant boundary terms, the dominant contribution to the integrals arises from one or more saddle points where the gradient of the function f in the exponent vanishes. The vicinity of the saddle point is characterized by the Hessian matrix containing second derivatives of f . While in leading order, only the determinant of the

Hessian matrix enters, the NTLO requires the knowledge of the inverse of the Hessian matrix. Therefore, before discussing the NTLO, we first need to analyze the Hessian matrix. Luckily, it will turn out that it allows for an analytical diagonalization in the problem at hand.

For the function f defined by (32) and (33), it is straightforward to calculate the gradient and to determine the saddle points. In fact, one can show that there exists a family of saddle points

$$\mathbf{k}_0 = \dots = \mathbf{k}_{r-1} \equiv \mathbf{k}_{\text{sp}} \quad (34)$$

parametrized by \mathbf{k}_{sp} . As a consequence, at the saddle points the scattering plane and the Fresnel planes coincide and we have $\chi^{(\text{in})} = \chi^{(\text{out})} = 0$ for each reflection at the sphere.

On the saddle-point manifold, the Hessian matrix can be brought into block-diagonal form

$$\mathbf{H} = \begin{pmatrix} \mathbf{H}_{xx} & 0 \\ 0 & \mathbf{H}_{yy} \end{pmatrix} \quad (35)$$

by arranging rows and columns in the order of $(k_{0,x}, \dots, k_{r-1,x}, k_{0,y}, \dots, k_{r-1,y})$. The matrix blocks are given by the second derivative of f evaluated at the saddle point

$$(\mathbf{H}_{xx})_{ij} = \left. \frac{\partial^2 f}{\partial k_{i,x} \partial k_{j,x}} \right|_{\text{sp}} \quad (36)$$

with a corresponding expression for \mathbf{H}_{yy} . Due to the block structure of the Hessian matrix, we can perform the integrations over the x - and y -components of the wave vectors separately.

The blocks of the Hessian matrix can be expressed as $\mathbf{H}_{xx} = \mathbf{H}_{yy} = (1/2\kappa_{\text{sp}})\Gamma_r$ with the $r \times r$ circulant matrix

$$\Gamma_r = \begin{pmatrix} 2 & -1 & & -1 \\ -1 & 2 & -1 & \\ & -1 & \ddots & \ddots \\ & & \ddots & \ddots & -1 \\ -1 & & & -1 & 2 \end{pmatrix} \quad (37)$$

where the matrix elements not shown are zero. κ_{sp} is obtained from \mathbf{k}_{sp} by means of the dispersion relation (5). In the special case of two round trips, we have

$$\Gamma_2 = \begin{pmatrix} 1 & -1 \\ -1 & 1 \end{pmatrix}, \quad (38)$$

while for $r = 1$ we have $f \equiv 0$.

It is now convenient to introduce transformed variables v through

$$k_{j,x} = \sum_{l=0}^{r-1} W_{jl} v_{l,x} \quad (39)$$

with

$$W_{jl} = \frac{1}{\sqrt{r}} \exp\left(\frac{2\pi i}{r} jl\right). \quad (40)$$

After the transformation, the blocks of the Hessian matrix are of counter-diagonal form

$$(\mathbf{W}^T \mathbf{H}_{xx} \mathbf{W})_{jl} = \lambda_j \delta_{j,r-l} \quad (41)$$

with the eigenvalues

$$\lambda_j = \frac{2}{\kappa_{\text{sp}}} \sin^2\left(\frac{\pi j}{r}\right) \quad (42)$$

and $j = 0, 1, \dots, r-1$. Since $\mathbf{H}_{xx} = \mathbf{H}_{yy}$, the same procedure is applied to the y -components as well.

Both blocks of the Hessian matrix contain one vanishing eigenvalue associated with the one-dimensional family of saddle points (34). As a consequence, the variables $v_{0,x}$ and $v_{0,y}$ need to be integrated out exactly. The remaining integrations over $v_{j,x}$ and $v_{j,y}$ with $j = 1, \dots, r-1$ can be evaluated within the saddle-point approximation up to NTLO as we will explain now.

If the sphere radius R provides the largest length scale, the integrals (30) are dominated by a region around the saddle point which scales with $R^{-1/2}$ in all directions except for the direction of the saddle-point family. In order to obtain the NTLO contribution, we thus need to expand the prefactor g up to second order around the saddle point while the function f appearing in the exponent needs to be expanded up to fourth order in deviations from the saddle point. Keeping the second-order term in the exponent and expanding the remaining exponential up to fourth order in the variables, we are left with integrands of Gaussian form multiplied by polynomials. Evaluating the corresponding integrals we find

$$\text{tr } \mathcal{M}^r = \frac{R}{2r} \int_{\xi/c}^{\infty} d\kappa_{\text{sp}} \kappa_{\text{sp}}^r \left[F_0 + \frac{1}{R} F_1 + o\left(R^{-1}\right) \right]. \quad (43)$$

In deriving this result, we made use of the fact that $f|_{\text{sp}} = 0$ and that the product of the non-vanishing eigenvalues (42) of the Hessian yields

$$\prod_{j=1}^{r-1} \frac{1}{\lambda_j} = \frac{(2\kappa_{\text{sp}})^{r-1}}{r^2}. \quad (44)$$

Finally, we transformed from the variables $v_{0,x}$ and $v_{0,y}$ back to the original wave vector at the saddle point and used (5) to express the integral in terms of κ_{sp} .

Up to NTLO, the integrand in (43) is specified by

$$F_0 = g|_{\text{sp}} \quad (45)$$

and

$$F_1 = g|_{\text{sp}} \left(\sum_{ijk} \frac{2f_{ijk}f_{\bar{i}\bar{j}\bar{k}} + 3f_{ij\bar{j}}f_{\bar{i}k\bar{k}}}{24\lambda_i\lambda_j\lambda_k} - \sum_{ij} \frac{f_{i\bar{i}j\bar{j}}}{8\lambda_i\lambda_j} \right) + \sum_{ij} \frac{g_{i\bar{i}j\bar{j}}}{2\lambda_i\lambda_j} + \sum_i \frac{g_{i\bar{i}}}{2\lambda_i}. \quad (46)$$

The eigenvalues λ_i have been defined in (42). For the indices, we use the short-hand notation $\bar{i} = r - i$ and the summation over the indices implies a summation also over the corresponding components x and y . Finally, the indices at the functions f and g denote derivatives with respect to the corresponding components of v evaluated at the saddle point.

A closer analysis reveals that two of the terms in (46) vanish because the functions f and g are symmetric with respect to their arguments. Let us consider the fourth term in (46) and specifically the first derivative

$$\left. \frac{\partial g}{\partial v_{i,x}} \right|_{\text{sp}} = \sum_{l=0}^{r-1} W_{il} \left. \frac{\partial g}{\partial k_{l,x}} \right|_{\text{sp}} \quad (47)$$

where $i \neq 0$, i.e. we are not taking a derivative along the saddle-point manifold. Because of the symmetry of g just mentioned, the derivative on the right-hand side evaluated at the saddle point is independent of l . The resulting sum over the Fourier factors (40) vanishes so that $g_i = 0$. Along the same lines one can show that $f_{ij\bar{j}} = 0$. Instead of (46), it is thus sufficient to evaluate

$$F_1 = g|_{\text{sp}} \left(\sum_{ijk} \frac{f_{ijk} f_{i\bar{j}\bar{k}}}{12\lambda_i \lambda_j \lambda_k} - \sum_{ij} \frac{f_{i\bar{i}\bar{j}\bar{j}}}{8\lambda_i \lambda_j} \right) + \sum_i \frac{g_{i\bar{i}}}{2\lambda_i}. \quad (48)$$

The results presented in this section take into account the corrections of order $1/R$ arising from the NTLO of the saddle-point approximation. However, it should be kept in mind that there is a second source of corrections of order $1/R$, namely the diffractive correction in the scattering amplitudes (22). In the following subsection, we will evaluate the leading term (45) in the saddle-point expansion and obtain already a part of the contributions to the NTLO Casimir term. The contributions arising from (48) will be discussed in the subsequent subsection.

B. Leading saddle-point contribution

At the saddle point, the projection of the wave vector onto the xy -plane does not change during the scattering at the sphere and thus the scattering plane and the Fresnel planes coincide. In particular, according to (21) the coefficients C and D vanish and polarization mixing does not contribute to leading order in the saddle-point approximation. As a consequence, the leading term F_0 in the integrand of (43) given by (45) can be decomposed as

$$g|_{\text{sp}} = g_{\text{TE}} + g_{\text{TM}} \quad (49)$$

where in view of (31)

$$g_p = \frac{\exp(-2\kappa_{\text{sp}} L r)}{\kappa_{\text{sp}}^r} \left(1 + \frac{r}{R} s_p|_{\text{sp}} \right). \quad (50)$$

Expression (50) results from a sequence of r reflections at the sphere with only one of them picking the diffractive correction. The contributions for TE and TM correspond to the terms with $p = \perp$ and $p = \parallel$ in (24), respectively, and can be expressed by means of (14) and (5) as

$$\begin{aligned} s_{\text{TE}}|_{\text{sp}} &= \frac{1}{\kappa_{\text{sp}}^3} \left(\frac{\xi^2}{2c^2} - \kappa_{\text{sp}}^2 \right) \\ s_{\text{TM}}|_{\text{sp}} &= -\frac{1}{\kappa_{\text{sp}}^3} \frac{\xi^2}{2c^2}. \end{aligned} \quad (51)$$

Carrying out the integral over κ_{sp} in (43), we find for the contributions of the two polarizations arising from F_0

$$\left(\text{tr } \mathcal{M}_{\text{TE}}^r \right)_0 = \frac{R}{L} \frac{e^{-u}}{4r^2} + \frac{1}{8} \left[(u^2 - 4) E_1(u) - (u - 1)e^{-u} \right] \quad (52)$$

and

$$\left(\text{tr } \mathcal{M}_{\text{TM}}^r \right)_0 = \frac{R}{L} \frac{e^{-u}}{4r^2} - \frac{1}{8} \left[u^2 E_1(u) - (u - 1)e^{-u} \right] \quad (53)$$

Here, $u = 2\xi L r / c$ and E_1 denotes the exponential integral function [48].

Evaluating the expression for the Casimir energy (8), we obtain

$$\mathcal{E}_{p,0} = \mathcal{E}_{\text{PFA}} \left(\frac{1}{2} + \beta_{d,p} \frac{L}{R} \right) \quad (54)$$

with

$$\beta_{d,\text{TE}} = -\frac{25}{2\pi^2} \quad (55)$$

$$\beta_{d,\text{TM}} = -\frac{5}{2\pi^2}. \quad (56)$$

The complete diffractive correction of order $1/R$ is thus quantified by

$$\beta_d = -\frac{15}{\pi^2}. \quad (57)$$

C. Geometric optical correction to PFA

In this section, we calculate the remaining part of the correction to PFA, i.e. the coefficient β_{go} . This contribution is due to the first correction of the saddle-point approximation with the integrand F_1 specified in (48). Since these terms are already of order $1/R$, we only need to take into account the leading-order term in the matrix elements (26) of the reflection operator. In other words, the subleading term in the matrix elements associated to diffraction does not contribute to order $1/R$ when computing the integral of F_1 in (43). Therefore, the term discussed in this section can be interpreted in terms of geometrical optics.

Introducing the angle $\chi = \chi^{(\text{in})} + \chi^{(\text{out})}$, we obtain from (19) and (26) to leading order

$$\begin{aligned} \rho_{\text{TM},\text{TM}} &= -\rho_{\text{TE},\text{TE}} = \cos(\chi) \\ \rho_{\text{TE},\text{TM}} &= \rho_{\text{TM},\text{TE}} = \sin(\chi). \end{aligned} \quad (58)$$

Since at the saddle points, scattering plane and Fresnel planes coincide, we have $\chi|_{\text{sp}} = 0$ as well as $\rho_{\text{TE},\text{TM}}|_{\text{sp}} = \rho_{\text{TM},\text{TE}}|_{\text{sp}} = 0$. In view of (31), a non-vanishing tilt between scattering plane and Fresnel planes can thus only enter through the last term in (48). However, this is not the case as we will show now.

In view of the trace in (30), the sequence of r scattering processes necessarily involves an even number of polarization changes. Since the derivatives in $g_{i\bar{i}}$ appearing in (48) have to be evaluated at the saddle point, the relevant terms either contain zero or two polarization-mixing matrix elements. The relevant polarization-dependent contribution in (31) thus reads

$$\begin{aligned} &\sum_{p_0, \dots, p_{r-1}} \prod_{j=0}^{r-1} (-1)^{p_j} \rho_{p_{j-1}, p_j} \\ &= \prod_{i=0}^{r-1} \cos(\chi_{i+1,i}) \left(1 - \sum_{j>l=0}^{r-1} \tan(\chi_{j+1,j}) \tan(\chi_{l+1,l}) \right) \end{aligned} \quad (59)$$

where $\chi_{j+1,j}$ describes the sum of the angles $\chi^{(\text{in})}$ and $\chi^{(\text{out})}$ for the j -th scattering process.

As a single derivative of (59) vanishes when evaluated at the saddle point, there are two contributions to $g_{i\bar{i}}$. In the first contribution, no derivative of (59) is taken. This term can then simply be replaced by a factor of 1 and does not account for a tilt between the scattering plane and the Fresnel planes. The second contribution potentially accounts for such a tilt and takes the form

$$\begin{aligned} &\left(\frac{\partial^2}{\partial v_{i,x} \partial v_{r-i,x}} \sum_{p_0, \dots, p_{r-1}} \prod_{j=0}^{r-1} (-1)^{p_j} \rho_{p_{j-1}, p_j} \right) \Big|_{\text{sp}} \\ &= - \sum_j \left(\frac{\partial \chi_{j+1,j}}{\partial v_{i,x}} \frac{\partial \chi_{j+1,j}}{\partial v_{r-i,x}} \right) \Big|_{\text{sp}} \\ &\quad - \sum_{j>l} \left(\frac{\partial \chi_{j+1,j}}{\partial v_{i,x}} \frac{\partial \chi_{l+1,l}}{\partial v_{r-i,x}} + \frac{\partial \chi_{j+1,j}}{\partial v_{r-i,x}} \frac{\partial \chi_{l+1,l}}{\partial v_{i,x}} \right) \Big|_{\text{sp}} \end{aligned} \quad (60)$$

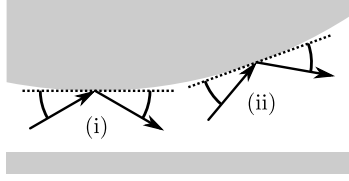


Fig. 3. Specular reflection at (i) a tangent plane at the bottom of the sphere and (ii) at a slightly tilted tangent plane.

where the first term arises from the second derivative of one of the cosine factors in (59), while the second term is obtained from single derivatives of two tangent factors. Combining the two sums allows us to express (60) as a product of two first derivatives of $\sum_{j=0}^{r-1} \chi_{j,j+1}$. As the latter quantity is symmetric in its arguments, its first derivative vanishes at the saddle point as demonstrated above. We conclude that the correction (48) arises only from scattering processes where the scattering plane is identical with the two Fresnel planes. The evaluation of (48) can thus be done as if there were no polarization mixing in the Fresnel polarization basis (3).

For the technical details of the remaining evaluation of (48), we refer the reader to the appendix. After integration over the saddle-point manifold, we find for the correction arising from F_1

$$\left(\text{tr } \mathcal{M}_p^r \right)_1 = -\frac{(r^2 - 1) \exp(-2Lr\tilde{\zeta}/c)}{12r^2} \quad (61)$$

which is independent of the polarization $p = \text{TE, TM}$. Carrying out the integration over imaginary frequencies $\tilde{\zeta}$ in (8), we obtain for the geometric optical correction

$$\beta_{\text{go}} = \frac{1}{3} - \frac{5}{\pi^2} \quad (62)$$

to which the two polarizations contribute equally.

As shown in [19], the PFA result corresponds to the leading term of the saddle-point approximation which arises from ray-optical specular reflection at the point of the sphere closest to the plate, i.e. scattering channel (i) in Fig. 3. The correction (62) can still be understood within geometrical optics but now the specular reflections may also occur at tangent planes slightly tilted with respect to the plate as illustrated by channel (ii) in Fig. 3.

D. Total leading order correction to PFA

The two contributions (57) and (62) are both negative and add up to the NTLO correction

$$\beta_1 = \frac{1}{3} - \frac{20}{\pi^2} \approx -1.693. \quad (63)$$

This result is known from the literature [36, 38] but now it has obtained a physical interpretation in terms of the relevant physical scattering processes. Furthermore, we have found that the contribution dominating by far is due to diffraction. According to table 1, diffraction contributes almost 90% to the reduction of the Casimir energy while specular reflection at a tangent plane inclined with respect to the plate contributes little over 10%. It is known that within the proximity force approximation, only a small effective area of radius $(RL)^{1/2}$ around the point of closest approach contributes to the Casimir energy (see for instance [19]). The rather small contribution from geometrical optics corrections implies that the effective area argument is barely

	TE	TM
diffraction	74.8%	15.0%
geometrical optics	5.1%	5.1%

Table 1. Relative contribution of the terms arising from diffraction and geometrical optics for the transverse electric (TE) and transverse magnetic (TM) polarization to the total correction of order $1/R$.

changed by the leading corrections. Curvature effects of the sphere manifest themselves mostly through diffraction.

The correction β_1 can also be split according to polarization. Keeping in mind that both polarizations contribute equally to β_{go} , we find from (55), (56), and (62) the contributions from the transverse electric modes

$$\beta_{\text{TE}} = \frac{1}{6} - \frac{15}{\pi^2} \approx -1.353 \quad (64)$$

and the transverse magnetic modes

$$\beta_{\text{TM}} = \frac{1}{6} - \frac{5}{\pi^2} \approx -0.339. \quad (65)$$

The TE contribution is thus about four times as large as the TM contribution.

In the literature, it has been noticed that the correction to the PFA coincides with the sum of two scalar field contributions, namely, Dirichlet-Dirichlet (DD) and Neumann-Neumann (NN) boundary condition [36, 38]. In this case, the individual contributions are given by

$$\beta_{\text{DD}} = \frac{1}{6} \quad (66)$$

and

$$\beta_{\text{NN}} = \frac{1}{6} - \frac{20}{\pi^2}. \quad (67)$$

Interestingly, this decomposition is not related to the physical mechanisms revealed in the present work.

5. CONCLUSIONS

We have derived the leading order correction to PFA in the plane-sphere geometry by developing the scattering formula in the plane wave basis. The momentum representation allows us to make a direct connection with geometrical optics and known results in semiclassical Mie scattering. Diffraction accounts for most of the total correction, with the TE polarization yielding a larger contribution than the TM one. The diffraction contribution is calculated to leading order in the saddle-point approximation, and it amounts to correcting the condition of geometric optical specular reflection at the tangent plane at the bottom of the sphere, i.e. scattering channel (i) in Fig. 3, by the leading order curvature effect.

The remaining part of the correction to PFA arises from the NTLO term in the saddle-point expansion, with the round-trip operator computed within the leading order WKB approximation. Such round trips correspond to a sequence of geometric optical specular reflections between plane and sphere, with the reflections at the latter taken at tangent planes which are slightly tilted with respect to the tangent plane at the bottom of the sphere, as illustrated by scattering channel (ii) in Fig. 3. Some of the scattering channels associated to a tilted tangent plane

allow for a mixing between TE and TM polarizations, provided that the scattering plane is also tilted with respect to the Fresnel plane as in the case shown in Fig. 2.

It is important to understand how polarization mixing channels contribute to the geometric optical correction to PFA since they are known to lead to negative Casimir entropies of geometrical origin [24–26, 49–51]. Although the polarization mixing matrix elements provide a non-vanishing contribution, the total correction associated to the tilt between the scattering and Fresnel planes turns out to vanish to NTLO. In other words, the final result for the leading order correction to PFA would be the same if the complications associated to the difference between the Fresnel and scattering polarization bases had been discarded from the beginning. Such remarks suggest that an alternative derivation, in which the polarization mixing effect would be entirely absent, would more directly lead to the leading order correction to PFA.

Funding. German Academic Exchange Service (DAAD); Coordination for the Improvement of Higher Education Personnel (CAPES-Brazil); Binational CAPES/DAAD PROBRAL collaboration program; National Council for Scientific and Technological Development (CNPq); National Institute of Science and Technology Complex Fluids (INCT-FCx); Research Foundations of the States of Minas Gerais (FAPEMIG), Rio de Janeiro (FAPERJ) and São Paulo (FAPESP) (2014/50983-3).

A. DERIVATION OF THE NEXT-TO-LEADING-ORDER TERM IN THE SADDLE-POINT EXPANSION

In this appendix, we present more details about the calculation of the NTLO term in the saddle-point approximation. More specifically, we calculate the contribution of the term

$$F_1 = g|_{\text{sp}} \left(\frac{D_1}{12} - \frac{D_2}{8} \right) + \frac{D_3}{2} \quad (68)$$

with

$$\begin{aligned} D_1 &= \sum_{\alpha, \beta, \gamma \in \{x, y\}} \sum_{i, j, l=1}^{r-1} \frac{1}{\lambda_i \lambda_j \lambda_l} \frac{\partial^3 f}{\partial v_{i, \alpha} \partial v_{j, \beta} \partial v_{l, \gamma}} \frac{\partial^3 f}{\partial v_{\bar{i}, \alpha} \partial v_{\bar{j}, \beta} \partial v_{\bar{l}, \gamma}} \\ D_2 &= \sum_{\alpha, \beta \in \{x, y\}} \sum_{i, j=1}^{r-1} \frac{1}{\lambda_i \lambda_j} \frac{\partial^4 f}{\partial v_{i, \alpha} \partial v_{\bar{i}, \alpha} \partial v_{j, \beta} \partial v_{\bar{j}, \beta}} \\ D_3 &= \sum_{\alpha \in \{x, y\}} \sum_{i=1}^{r-1} \frac{1}{\lambda_i} \frac{\partial^2 g}{\partial v_{i, \alpha} \partial v_{\bar{i}, \alpha}}, \end{aligned} \quad (69)$$

where we made use of the notation $\bar{i} = r - i$ introduced in Section 4A.

In the following, we demonstrate the calculation of the most complex term D_1 . The other terms can be computed analogously. After employing the chain rule, D_1 can be written as

$$D_1 = \sum_{p, q=0}^{r-1} \sum_{m, n, s=p}^{p+1} \sum_{t, u, w=q}^{q+1} a(m-t) a(n-u) a(s-w) \times d_{pq}(m, n, s; t, u, w) \quad (70)$$

where

$$a(s) = \frac{1}{r} \sum_{j=1}^{r-1} \frac{e^{2\pi i j s / r}}{\lambda_j} \quad (71)$$

and

$$d_{pq}(m, n, s; t, u, w) = \sum_{\alpha, \beta, \gamma \in \{x, y\}} \frac{\partial^3 \eta_{p, p+1}}{\partial k_{m, \alpha} \partial k_{n, \beta} \partial k_{s, \gamma}} \frac{\partial^3 \eta_{q, q+1}}{\partial k_{t, \alpha} \partial k_{u, \beta} \partial k_{w, \gamma}}. \quad (72)$$

Using the identity [52]

$$\sum_{j=1}^{r-1} \frac{e^{2\pi i j s / r}}{\sin^2(\pi j / r)} = \frac{1}{3} (r^2 - 6|s|r + 6s^2 - 1), \quad (73)$$

the function a evaluates to

$$a(s) = \frac{\kappa_{\text{sp}}}{6r} (r^2 - 6sr + 6s^2 - 1). \quad (74)$$

In view of its definition through a Fourier series, this function should be understood as r -periodic with $0 \leq s \leq r$.

The sum over the indices m, n and s in (70) runs only over p and $p+1$ since all other partial derivatives in (72) vanish. For the same reason the indices t, u and w take only the values q and $q+1$. Thus, we sum over 64 different arguments of the function d_{pq} . However, there are only three classes of arguments for which d_{pq} yields a non-zero value. These are given by

$$\begin{aligned} d_{pq}(p, p, p; q, q, q) &= d \\ d_{pq}(p+1, p, p; q, q, q) &= d_{pq}(p, p, p; q+1, q, q) = -\frac{d}{3} \\ d_{pq}(p+1, p, p; q+1, q, q) &= \frac{d}{3} \end{aligned} \quad (75)$$

with

$$d = \frac{3}{4} \frac{\kappa_{\text{sp}}^2}{\kappa_{\text{sp}}^6}. \quad (76)$$

On the other hand

$$d_{pq}(p+1, p, p; q, q+1, q) = d_{pq}(p+1, p, p; q, q, q+1) = 0. \quad (77)$$

All other sets of arguments can be reduced to the forms given by means of the following rules. In each triple of arguments one can perform the replacement $p \leftrightarrow p+1$ and/or $q \leftrightarrow q+1$ because the derivatives are evaluated at a saddle point. In this way, at most one argument is $p+1$ or $q+1$. Furthermore, because of commutativity of the partial derivatives, one can permute the two triples of arguments. However, this permutation has to be done in the same way on both triples as the derivatives are coupled through the indices α, β , and γ in (72). In this way, the argument $p+1$, if it exists, can be brought to the first position and we end up with one of the sets of arguments given above.

Taking these rules into account, (70) can be expressed as

$$D_1 = \sum_{p, q=0}^{r-1} A(p-q) \quad (78)$$

with

$$\begin{aligned} A(s) &= d \left(6a^3(s) + [a(s-1) + a(s+1)] \right. \\ &\quad \times \left. [a(s-1)a(s+1) - 4a^2(s)] \right). \end{aligned} \quad (79)$$

The resulting sum over polynomials can be evaluated and one finds

$$D_1 = \frac{(r-2)(r-1)^2(c^2\kappa_{\text{sp}}^2 - \zeta^2)}{rc^2\kappa_{\text{sp}}^3}. \quad (80)$$

The calculation for D_2 and D_3 is analogous but simpler. Note, however, that in contrast to (75) the various types of contributions do not necessarily differ simply by a numerical factor. Carrying out the calculation, one finds

$$D_2 = \frac{2(r-1)^2 \left((r-2)c^2\kappa_{\text{sp}}^2 - 3r\zeta^2 \right)}{3rc^2\kappa_{\text{sp}}^3} \quad (81)$$

and

$$D_3 = -\frac{(r^2-1) \left(\zeta^2 + L\kappa_{\text{sp}}(c^2\kappa_{\text{sp}}^2 + \zeta^2) \right)}{3c^2\kappa_{\text{sp}}^3} g|_{\text{sp}}. \quad (82)$$

We recall that according to our discussion in Sec. 4C the evaluation of D_3 has to be done for $\chi = 0$.

The total NTLO term in the saddle-point expansion thus is given by

$$F_1 = -\frac{(r^2-1) \left(rL\kappa_{\text{sp}}(c^2\kappa_{\text{sp}}^2 + \zeta^2) + \zeta^2 \right)}{6rc^2\kappa_{\text{sp}}^3} g|_{\text{sp}}. \quad (83)$$

REFERENCES

1. H. B. G. Casimir, "On the attraction between two perfectly conducting plates," *Proc. K. Ned. Akad. Wet.* **51**, 793 (1948).
2. M. Bordag, G. L. Klimchitskaya, U. Mohideen, and V. M. Mostepanenko, *Advances in the Casimir Effect* (Oxford University Press, 2009).
3. G. L. Klimchitskaya, U. Mohideen, and V. M. Mostepanenko, "The Casimir force between real materials: Experiment and theory," *Rev. Mod. Phys.* **81**, 1827 (2009).
4. R. Decca, V. Aksyuk, and D. López, "Casimir Force in Micro and Nano Electro Mechanical Systems," *Lect. Notes Phys.* **834**, 287 (2011).
5. S. K. Lamoreaux, "Progress in Experimental Measurements of the Surface-Surface Casimir Force: Electrostatic Calibrations and Limitations to Accuracy," *Lect. Notes Phys.* **834**, 219 (2011).
6. A. O. Sushkov, W. J. Kim, D. A. R. Dalvit, and S. K. Lamoreaux, "Observation of the thermal Casimir force," *Nat. Phys.* **7**, 230 (2011).
7. G. Torricelli, I. Pirozhenko, S. Thornton, A. Lambrecht, and C. Binns, "Casimir force between a metal and a semimetal," *EPL* **93**, 51001 (2011).
8. C.-C. Chang, A. A. Banishev, R. Castillo-Garza, G. L. Klimchitskaya, V. M. Mostepanenko, and U. Mohideen, "Gradient of the Casimir force between Au surfaces of a sphere and a plate measured using an atomic force microscope in a frequency-shift technique," *Phys. Rev. B* **85**, 165443 (2012).
9. D. Garcia-Sanchez, K. Y. Fong, H. Bhaskaran, S. Lamoreaux, and H. X. Tang, "Casimir Force and *In Situ* Surface Potential Measurements on Nanomembranes," *Phys. Rev. Lett.* **109**, 027202 (2012).
10. A. A. Banishev, G. L. Klimchitskaya, V. M. Mostepanenko, and U. Mohideen, "Demonstration of the Casimir Force between Ferromagnetic Surfaces of a Ni-Coated Sphere and a Ni-Coated Plate," *Phys. Rev. Lett.* **110**, 137401 (2013).
11. M. Sedighi, V. B. Svetovoy, and G. Palasantzas, "Casimir force measurements from silicon carbide surfaces," *Phys. Rev. B* **93**, 085434 (2016).
12. G. Bimonte, D. López, and R. S. Decca, "Isoelectronic determination of the thermal Casimir force," *Phys. Rev. B* **93**, 184434 (2016).
13. M. Elzbieciak-Wodka, M. N. Popescu, F. J. M. Ruiz-Cabello, G. Trefalt, P. Maroni, and M. Borkovec, "Measurements of dispersion forces between colloidal latex particles with the atomic force microscope and comparison with Lifshitz theory," *J. Chem. Phys.* **140**, 104906 (2014).
14. D. S. Ether jr. *et al.*, "Probing the Casimir force with optical tweezers," *EPL* **112**, 44001 (2015).
15. J. L. Garrett, D. A. T. Somers, and J. N. Munday, "Measurement of the Casimir Force between Two Spheres," *Phys. Rev. Lett.* **120**, 040401 (2018).
16. H.-J. Butt and M. Kappl, *Surface and Interfacial Forces* (Wiley-VCH Verlag, 2010).
17. B. Derjaguin, "Untersuchungen über die Reibung und Adhäsion, IV – Theorie des Anhaftens kleiner Teilchen," *Kolloid-Zs.* **69**, 155 (1934).
18. V. A. Parsegian, *Van der Waals Forces: A Handbook for Biologists, Chemists, Engineers, and Physicists* (Cambridge University Press, 2006).
19. B. Spreng, M. Hartmann, V. Henning, P. A. Maia Neto, and G.-L. Ingold, "Proximity force approximation and specular reflection: Application of the WKB limit of Mie scattering to the Casimir effect," *Phys. Rev. A* **97**, 062504 (2018).
20. M. Hartmann, G.-L. Ingold, and P. A. Maia Neto, "Advancing numerics for the Casimir effect to experimentally relevant aspect ratios," *Phys. Scr.* **93**, 114003 (2018).
21. P. A. Maia Neto, A. Lambrecht, and S. Reynaud, "Casimir energy between a plane and a sphere in electromagnetic vacuum," *Phys. Rev. A* **78**, 012115 (2008).
22. T. Emig, "Fluctuation-induced quantum interactions between compact objects and a plane mirror," *J. Stat. Mech.* (2008) P04007.
23. A. Canaguier-Durand, P. A. Maia Neto, I. Cervero-Pelaez, A. Lambrecht, and S. Reynaud, "Casimir Interaction between Plane and Spherical Metallic Surfaces," *Phys. Rev. Lett.* **102**, 230404 (2009).
24. A. Canaguier-Durand, P. A. Maia Neto, A. Lambrecht, and S. Reynaud, "Thermal Casimir Effect in the Plane-Sphere Geometry," *Phys. Rev. Lett.* **104**, 040403 (2010).
25. A. Canaguier-Durand, P. A. Maia Neto, A. Lambrecht, and S. Reynaud, "Thermal Casimir effect for Drude metals in the plane-sphere geometry," *Phys. Rev. A* **82**, 012511 (2010).
26. R. Zandi, T. Emig, and U. Mohideen, "Quantum and thermal Casimir interaction between a sphere and a plate: Comparison of Drude and plasma models," *Phys. Rev. B* **81**, 195423 (2010).
27. A. Lambrecht, P. A. Maia Neto, and S. Reynaud, "The Casimir effect within scattering theory," *New J. Phys.* **8**, 243 (2006).
28. T. Emig, N. Graham, R. L. Jaffe, and M. Kardar, "Casimir Forces Between Arbitrary Compact Objects," *Phys. Rev. Lett.* **99**, 170403 (2007).
29. M. Hartmann, G.-L. Ingold, and P. A. Maia Neto, "Plasma versus Drude Modeling of the Casimir Force: Beyond the Proximity Force Approximation," *Phys. Rev. Lett.* **119**, 043901 (2017).
30. M. Schaden and L. Spruch, "Infinity-free semiclassical evaluation of Casimir effects," *Phys. Rev. A* **58**, 935 (1998).
31. R. L. Jaffe and A. Scardicchio, "Casimir Effect and Geometric Optics," *Phys. Rev. Lett.* **92**, 070402 (2004).
32. A. Scardicchio and R. L. Jaffe, "Casimir effects: an optical approach I. Foundations and examples," *Nucl. Phys. B* **704**, 552 (2005).
33. H. M. Nussenzveig, *Diffraction Effects in Semiclassical Scattering* (Cambridge University Press, 1992).
34. W. T. Grandy Jr., *Scattering of Waves from Large Spheres* (Cambridge University Press, 2005).
35. M. Bordag and V. Nikolaev, "Casimir force for a sphere in front of a plane beyond proximity force approximation," *J. Phys. A: Math. Theor.* **41**, 164002 (2008).
36. L. P. Teo, M. Bordag, and V. Nikolaev, "Corrections beyond the proximity force approximation," *Phys. Rev. D* **84**, 125037 (2011).
37. C. D. Fosco, F. C. Lombardo, and F. D. Mazzitelli, "Proximity force approximation for the Casimir energy as a derivative expansion," *Phys. Rev. D* **84**, 105031 (2011).
38. G. Bimonte, T. Emig, R. L. Jaffe, and M. Kardar, "Casimir forces beyond the proximity approximation," *EPL* **97**, 50001 (2012).
39. L. P. Teo, "Material dependence of Casimir interaction between a sphere and a plate: First analytic correction beyond proximity force approximation," *Phys. Rev. D* **88**, 045019 (2013).
40. G. Bimonte, T. Emig, and M. Kardar, "Material dependence of Casimir forces: Gradient expansion beyond proximity," *Appl. Phys. Lett.* **100**, 074110 (2012).
41. M. Bordag and I. Pirozhenko, "Vacuum energy between a sphere and a plane at finite temperature," *Phys. Rev. D* **81**, 085023 (2010).
42. G. Bimonte and T. Emig, "Exact Results for Classical Casimir Interactions: Dirichlet and Drude Model in the Sphere-Sphere and Sphere-Plane Geometry," *Phys. Rev. Lett.* **109**, 160403 (2012).

43. C. D. Fosco, F. C. Lombardo, and F. D. Mazzitelli, "Derivative expansion for the electromagnetic Casimir free energy at high temperatures," *Phys. Rev. D* **92**, 125007 (2015).
44. G. Bimonte, "Classical Casimir interaction of perfectly conducting sphere and plate," *Phys. Rev. D* **95**, 065004 (2017).
45. M. Nieto-Vesperinas, *Scattering and Diffraction in Physical Optics* (World Scientific, 2006).
46. C. F. Bohren and D. R. Huffman, *Absorption and Scattering of Light by Small Particles* (Wiley, New York, 1983).
47. H. M. Nussenzveig, "High-Frequency Scattering by a Transparent Sphere. I. Direct Reflection and Transmission," *J. Math. Phys.* **10**, 82 (1969).
48. NIST Digital Library of Mathematical Functions. <http://dlmf.nist.gov/6.2>, Release 1.0.20 of 2018-09-15. F. W. J. Olver, A. B. Olde Daalhuis, D. W. Lozier, B. I. Schneider, R. F. Boisvert, C. W. Clark, B. R. Miller, and B. V. Saunders, eds.
49. K. A. Milton, R. Gu  rout, G.-L. Ingold, A. Lambrecht, S. Reynaud, "Negative Casimir entropies in nanoparticle interactions," *J. Phys.: Condens. Matter* **27**, 214003 (2015).
50. G.-L. Ingold, S. Umrath, M. Hartmann, R. Gu  rout, A. Lambrecht, S. Reynaud, and K. A. Milton, "Geometric origin of negative Casimir entropies: A scattering-channel analysis," *Phys. Rev. E* **91**, 033203 (2015).
51. S. Umrath, M. Hartmann, G.-L. Ingold, and P. A. Maia Neto, "Disentangling geometric and dissipative origins of negative Casimir entropies," *Phys. Rev. E* **92**, 042125 (2015).
52. B. C. Berndt and B. P. Yeap, "Explicit evaluations and reciprocity theorems for finite trigonometric sums," *Adv. Appl. Math.* **29**, 358 (2002).